Elastic strains in GaAs/AlAs quantum dots studied by high-resolution x-ray diffraction

Elastic strains in GaAs/AlAs quantum dots studied by high-resolution x-ray diffraction

V. Holý,* A. A. Darhuber, and G. Bauer
Institut für Halbleiterphysik, Johannes Kepler Universität, A-4040 Linz, Austria

P. D. Wang, Y. P. Song, C. M. Sotomayor Torres, and M. C. Holland
Nanoelectronics Research Center, Department of Electronics and Electrical Engineering, University of Glasgow, Glasgow G12 8QQ, United Kingdom
(Received 30 January 1995)

We have studied a GaAs/AlAs periodic quantum dot array (fabricated by electron beam lithography and reactive ion etching) using high-resolution x-ray reciprocal space mapping around the (004) and $(\bar{1}\bar{1}3)$ reciprocal lattice points. Both the coherently and the diffusely scattered x-ray intensities were analyzed by performing two-dimensional model calculations and comparing them with the measured reciprocal space maps of the diffracted intensity. From the distribution of the diffracted intensities we deduced the average strain status in the dots. From the numerical simulations it is evident that random elastic strain fields are present, which extend through almost the whole volume of the quantum dot. The simulations of the x-ray measurements revealed that the crystalline part of the dots is considerably smaller as scanning electron micrographs would indicate, namely, 50 nm instead of 65 nm, respectively.

I. INTRODUCTION

Quantum wires and quantum dots have been predicted to exhibit unique optical and electrical properties. Quantum wire lasers were expected to show a significantly lower threshold current than two-dimensional quantum well laser, the luminescence efficiency of quantum dots should be even higher. The performance of real, etched nanostructures often does not come up to the expectations.[1] The most probable reason for this fact is that the etching process induces deep electronic traps, which act as nonradiative recombination centers, up to a distance of several nanometers away from the surface. During the etching, structural defects are introduced into a layer at the sidewalls of the wires or dots, and the perfection of the crystal lattice in the wires and dots is diminished, due to random strains propagating from these defects. Such random strain fields may be decisive for the electrical and optical properties of laterally patterned quantum confined systems.

Moreover, the crystal lattice in the dot is inhomogeneously strained, mainly due to the internal stresses in the multilayer structure, in which the dot array is fabricated. These stresses are relieved during patterning, which leads to elastic strain relaxation[2] deforming significantly the crystal lattice in the dots. Another source of nonrandom inhomogeneous strains is the lattice expansion, due to foreign interstitial atoms or vacancies incorporated into the dots during the etching process.

Both the nonrandom and the random strains can be studied by x-ray diffraction. Several groups demonstrated the applicability of x-ray diffraction for the structural characterization of periodic quantum wires and quantum dots in the past years.[3–6] Emphasis was laid on nonrandom strains, which may cause shifts or deformations of the maxima of the diffracted intensity distribution in reciprocal space. To our knowledge, the random strains in wire and dot structures have not been studied so far. These strains give rise to incoherent (diffuse) x-ray scattering that can be studied by means of the reciprocal space mapping method.[7,8]

It is well-established[9–11] that the distribution of the diffusely scattered intensity in reciprocal space yields information on the correlation properties of the random deformation field. From the symmetry of this distribution, the nature of the structural defects can be deduced, the quantitative comparison of the diffuse intensity with the diffraction theory yields an estimate of their density.[10] If the density of the structural defects is sufficiently high, the statistical distribution of the random strains is Gaussian.[9] Then, the shapes of the diffuse scattering peaks are Gaussian as well, and the parameters of these random strains can easily be found using the random strain tensor model.[11]

In the case of laterally patterned structures, the reciprocal space distribution of the diffusely scattered intensity is affected by the shapes of the scattering regions. This fact makes it possible to determine the size and the form of randomly strained regions in the dots.

There is a vast amount of literature on indirect observations of changes of the strain status and damage introduced by nanofabrication techniques from measurements of electronic and optical properties of low dimensional systems.[12–14] Already in 1989, Clausen *et al.*[15] investigated the normalized cathodoluminescence intensity of GaAs/$Al_xGa_{1-x}As$ quantum dots as a function of the dot radius. The luminescence intensity was found to decrease by several orders of magnitude when the

dot radius fell below 500 nm. On the other hand, in nonetched one-dimensional $GaAs/Ga_{1-x}Al_xAs$ structures, where the quantum confinement was induced by a properly etched $In_xGa_{1-x}As$ stressor,[16,17] a decrease of the integrated photoluminescence intensity was observed, but less dramatic than previously found in etched structures. Furthermore, it was found that annealing of dry etched $GaAs/Al_xGa_{1-x}As$ quantum dots[18] leads to a strong recovery of integrated photoluminescence by at least one order of magnitude for all dot sizes, which indicates that structural defects are introduced by this fabrication technique. Wang *et al.*[19,20] characterized GaAs nanostructures using Raman scattering and found that a damaged layer with a thickness of approximately 35 nm is still crystalline.

In this paper, we report about x-ray reciprocal space mapping investigations of dry etched GaAs/AlAs quantum dots regarding both the coherently and incoherently scattered x-ray wave fields. From the coherent part, we deduced the strain status of the etched multiple quantum well and proved the existence of a completely nondiffracting (i.e., probably heavily distorted) layer at the sidewalls of the dots. The measurement of the diffuse (incoherent) x-ray intensity diffracted from a dot array is reported. From the reciprocal space maps of the diffuse scattering, we found evidence for the presence of random elastic strain fields, which extend through nearly the whole quantum dot and we estimated the mean square deviations of these strains.

In Sec. II, the fabrication procedure of the samples and the experimental setup are introduced. In Sec. III, the experimental data are presented. Section IV describes the theory, on which the simulations are based. The results of the theoretical analysis are discussed in Sec. V. A summary is given in Sec. VI, the conclusions.

II. EXPERIMENT

The GaAs/AlAs quantum dots have been fabricated by nanostructuring a 30 period AlAs/GaAs multiple quantum well (MQW) deposited on a 1 μm GaAs buffer. The 8.2 nm thick GaAs wells are separated by 13.1 nm AlAs barriers resulting in a total thickness of $H_1 = 639$ nm. The MQW was capped by a 20 nm GaAs layer. The whole structure was grown on a GaAs (001) substrate on top of which 25 periods of a 5 ML/5 ML short period GaAs/AlAs superlattice have been deposited. The lithography was done with a Leica Cambridge EBPG5-HR electron beam pattern generator. The dots have been prepared by magnetically confined plasma reactive ion etching,[21] using NiCr metal masks, and the etching gases $SiCl_4$ with a flow rate of 13.5 SCCM (where SCCM denotes cubic centimeter per minute at STP) and O_2 with a flow rate of 1.5 SCCM. The operating pressure was 0.5 mTorr. The microwave power was 54 W, the rf power 35 W and the resulting dc bias was -230 V. A scanning electron micrograph of an equivalently fabricated dot array has previously been published.[21]

The etch depth was approximately 900 nm, consequently, about $H_2 = 250$ nm of the GaAs buffer have been structured into dots as well (see Fig. 1). The short period superlattice below the GaAs buffer was not etched and will not be considered further. The dot array is oriented along [110] and [1$\bar{1}$0] directions and has rectangular symmetry. In the [110] direction, the dot period d was nominally 300 nm, in the perpendicular direction 350 nm (see Fig. 1). From scanning electron microscopy micrographs, we deduced a dot radius of 65 nm, the structural inhomogeneities can cause a deviation of this value by ± 5 nm. The total structured area is about 26 mm^2. Such comparatively large areas are necessary for an acceptable signal-to-noise ratio, if the x-ray experiments are performed with standard laboratory equipment.

We used a Philips MRD diffractometer with a four crystal Ge (220) monochromator and a channel cut two crystal Ge (220) analyzer with an angular resolution of 12 arc seconds. A conventional fixed copper anode with a power consumption of 1.6 kW and Cu $K\alpha_1$ radiation ($\lambda = 1.540\,59$ Å) was used. The independent variation of the two diffraction angles ω (between incident x rays and sample surface) and 2θ (between incident and scattered x rays) provides the possibility of reciprocal space mapping, i.e., the acquisition of two-dimensional projections in the three-dimensional reciprocal space.[7,8]

III. RECIPROCAL SPACE MAPPING

The situation in reciprocal space is sketched in Fig. 2(a) for the diffraction geometry chosen. The allowed reflections of GaAs are depicted as crosses "×." The shaded circles labeled with "Laue" are not accessible for x-ray diffraction in Bragg (reflection) geometry, because either the entrance angle ω, or the exit angle is smaller than 0°. The incident x-ray wave vector is $\mathbf{k}_i$, $\mathbf{k}_s$ is the wave vector of the diffracted x rays, and $\mathbf{h}$ is the corresponding reciprocal space vector. If, as in the present case, the epitaxial layer system is periodic in the growth direction, the "conventional" reciprocal lattice peaks are accompanied by a series of satellite peaks in this direction. In the case of a superlattice, they are called superlattice satellites, hence they are labeled with "SL_i." Their spacing is constant and given by the inverse of the multiple quantum well period. If an additional lateral periodicity is embossed onto the system by means of, for example, reactive ion etching, the multiple quantum

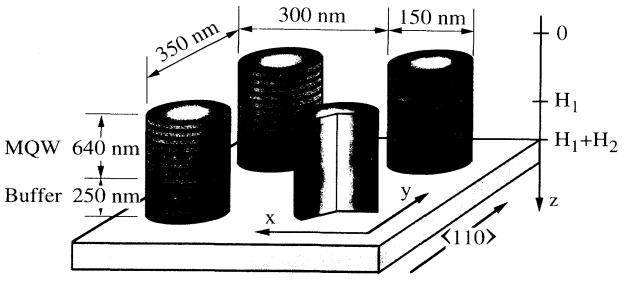

FIG. 1. Schematic diagram of the periodic GaAs/AlAs dot array.

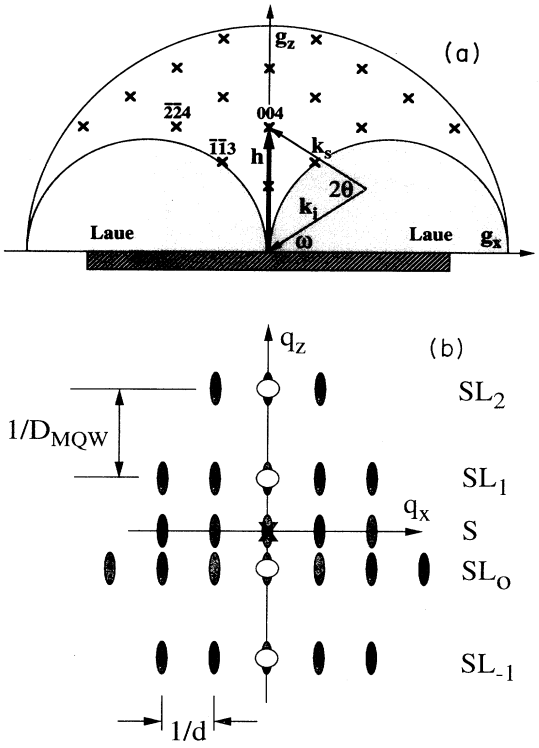

FIG. 2. (a) Schematic diagram of accessible part of reciprocal space for Bragg (reflection) geometry. Crosses denote the reciprocal lattice points of the zinc blende structure. Coordinate system: $g_x \| [110]$, $g_z \| [001]$. (b) Positions of the superlattice satellites SL_i (open circles) and dot satellites (shaded ellipses) shown schematically around (004). D_{MQW} denotes the period of the multiple quantum well in growth direction and d is the period of the dot array in the diffraction plane.

well peaks exhibit satellites in the *lateral* direction as well. These so-called dot satellites are also periodic in reciprocal space, their spacing again is given by the inverse of the real space period d. Figure 2(b) illustrates the situation close to the GaAs (004) reflection. Because of the different lattice constants of GaAs ($a_{GaAs} = 5.653\,25$ Å) and AlAs ($a_{AlAs} = 5.660$ Å), the zeroth order multiple quantum well peak is shifted along the growth direction. Its position is determined by the lattice parameters and the layer thicknesses of the MQW structure.

The measured reciprocal space maps (RSM's, $q_x \| [110]$, $q_z \| [001]$) of the quantum dot array around the GaAs (004) and ($\bar{1}\bar{1}3$) reflection are shown in Figs. 3(a) and 4(a), respectively, where isointensity contours are plotted. The RSM around (004) has been measured using the channel-cut analyzer in front of the detector, whereas that of ($\bar{1}\bar{1}3$) (small exit angle) has been acquired with a narrow slit, which was necessary for sufficient signal-to-noise ratio. We have chosen the ($\bar{1}\bar{1}3$) diffraction, because it is the most intense asymmetric diffraction for our setup. The model calculations shown in Figs. 3(b) and 4(b) will be discussed later. The upper part of the RSM stems from the substrate part of the dots, the lower part from the multiple quantum well. The lengthy streak through the substrate peak with the coordinates $q_x = q_z = 0$ is an artifact, the so-called analyzer streak.[8]

The overall geometrical perfection of the rectangular dot array in the sample studied is evident from the large number of dot satellites (10) observed both for (004) and ($\bar{1}\bar{1}3$) diffractions. Another striking feature of these reciprocal space maps is the occurrence of a broad peak of diffuse scattering both at ($\bar{1}\bar{1}3$) and at (004), a feature, which to our knowledge has not been considered previously. The shape of the isointensity contours, due to diffuse scattering, which accompanies both the (004) and ($\bar{1}\bar{1}3$) SL_0 maxima, is approximately elliptical. For the ($\bar{1}\bar{1}3$) diffraction, its main axis is notably rotated with respect to the q_x-[110] direction.

Whereas the dot satellites stem from strictly periodic atomic arrangements, which are the same for more or less all quantum dots, the diffuse scattering originates from random strains, which show no correlation in any two different dots. The theoretical description of such diffraction patterns, both the coherent and the diffuse parts is given in Sec. IV.

IV. THEORETICAL DESCRIPTION

In this section, we derive formulas for the simulation of the RSM's taking into account both the coherent and

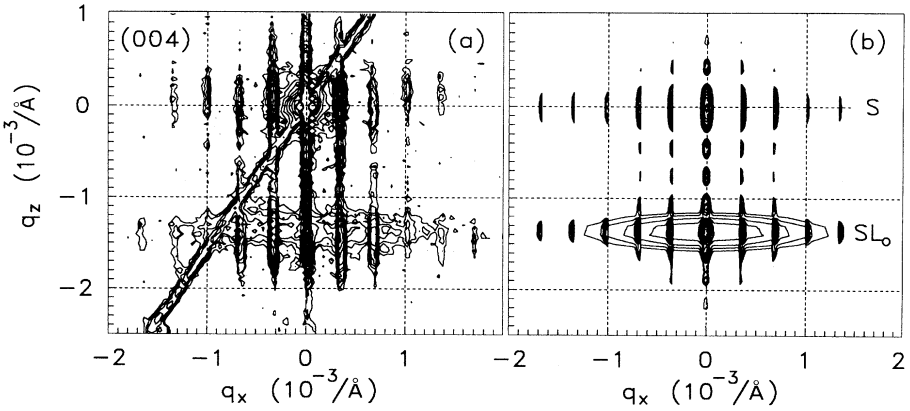

FIG. 3. Measured (a) and calculated (b) reciprocal space maps of the dot array close to the (004) substrate reciprocal lattice point. The intensity scale is logarithmic, the step between two isointensity contours is $\Delta \log_{10}(I) = 0.2$. In part (b), "$S$" and "$SL_0$" denote the diffracted intensities originating from the substrate and MQW parts, respectively.

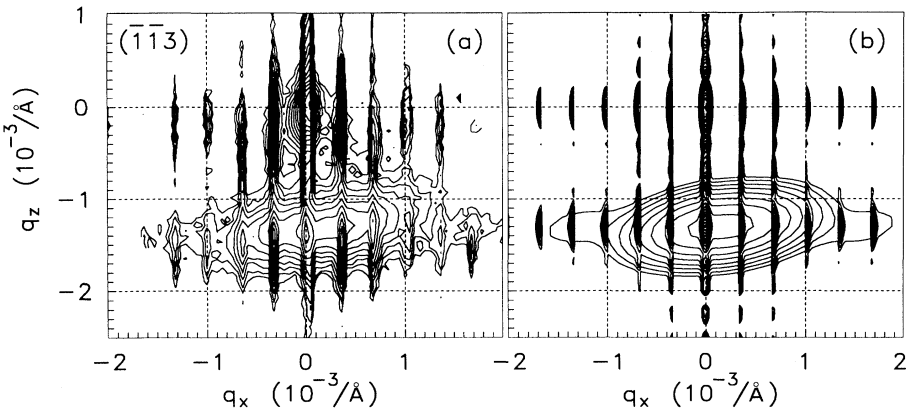

FIG. 4. Same as in Fig. 3, close to the reciprocal lattice point $(\bar{1}\bar{1}3)$ (low angle of exit).

the diffuse components of the diffracted intensity from the dot pattern. For this description, we use the kinematical approximation. As shown by Gailhanou *et al.*,[22] the possible dynamical features occur only along the analyzer and monochromator streaks. Furthermore, dynamical diffraction is rather important for the description of the scattering from the corrugated buffer and not from the MQW part of the dots.

We have chosen the y axis parallel to the sample surface and perpendicular to the diffraction plane defined by the incident and diffracted x-ray wave vectors. $\mathbf{r}_{\|} = (x, y)$ denotes the in-plane component of the position vector $\mathbf{r}$, the x axis is parallel both to the sample surface and the diffraction plane, the z axis is parallel to the inward normal of the surface. The plane $z = 0$ coincides with the sample surface (see Fig. 1). Distances in reciprocal space are measured relative to the GaAs substrate peak, consequently, the reciprocal space vectors $\mathbf{q}$ have their origin in the reciprocal lattice point of the substrate [see Fig. 2(b)].

The dots consist of two parts. The upper part with height H_1 has the multiple quantum well structure, the lower "neck" (with height H_2) is due to the etching into the buffer (see Fig. 1). The diffracted amplitude is proportional to the hth Fourier coefficient χ_h of the crystal polarizability. For $z < H_1$, the polarizability coefficient χ_h is a periodic function of the vertical coordinate z. This function can be expressed by means of a Fourier series and its maxima are represented by a row of vertical satellite reciprocal lattice points along the q_z axis as shown in Fig. 2(b). In the following, we will only investigate the region close to the zero-order vertical multiple quantum well satellite SL_0. Thus, from the viewpoint of diffraction, the multiple quantum well structure is equivalent to a homogeneous crystalline layer with an averaged polarizability coefficient. Then, the actual polarizability profile $\chi_h(z)$ is replaced by its mean value χ_h^{MQW} in the multiple quantum well and by χ_h^{sub} in the substrate part of the dots, so that it can be defined by

$$\chi_h(z) = \chi_h^{\mathrm{MQW}} H_{\mathrm{MQW}}(z) + \chi_h^{\mathrm{sub}} H_{\mathrm{sub}}(z), \tag{1}$$

where $H_{\mathrm{MQW}}(z) = 1$ for $z \in (0, H_1)$ and $H_{\mathrm{sub}}(z) = 1$ for $z \in (H_1, H_1 + H_2)$, and zero elsewhere. The shape of the quantum dots is described by the shape function,

$$\Omega(\mathbf{r}) = \begin{cases} 1 & \text{in the dots} \\ 0 & \text{elsewhere.} \end{cases} \tag{2}$$

The positions of the dots form a rectangular two-dimensional array parallel to the x and y axes, the array vectors are denoted $\mathbf{R}$. If we assume that the dots have perfectly vertical sidewalls, the block shape function can be decomposed into a vertical and an in-plane components as follows:

$$\Omega(\mathbf{r}) = \Omega_{\|}(\mathbf{r}_{\|})[H_{\mathrm{MQW}}(z) + H_{\mathrm{sub}}(z)] \tag{3}$$

and the in-plane component is

$$\Omega_{\|}(\mathbf{r}_{\|}) = \sum_{\mathbf{R}} \Omega_D(\mathbf{r}_{\|} - \mathbf{R}). \tag{4}$$

We express the in-plane component of the shape function as a sum of in-plane components Ω_D of the shape functions of the individual dots at the positions $\mathbf{R}$. We assume that the shape of the dots is a cylinder with radius R_D, thus, the in-plane shape function of an individual dot is

$$\Omega_D(\mathbf{r}_{\|}) = \begin{cases} 1 & \text{for } |\mathbf{r}_{\|}| < R_D \\ 0 & \text{elsewhere.} \end{cases} \tag{5}$$

Since $\Omega_{\|}$ is periodic, it can be expressed as a Fourier series over the reciprocal array with the array vectors $\mathbf{G}$,

$$\Omega_{\|}(\mathbf{r}_{\|}) = \sum_{\mathbf{G}} \Omega_D^{\mathrm{FT}}(\mathbf{G}) \exp(-2\pi i \mathbf{G} \cdot \mathbf{r}_{\|}), \tag{6}$$

the superscript FT denotes the Fourier transformation.

In kinematical approximation, the strain field in the dots $\mathbf{u}(\mathbf{r})$ influences the phase of the diffracted radiation by means of the function Ψ,

$$\Psi(\mathbf{r}) = \exp[2\pi i \mathbf{h} \cdot \mathbf{u}(\mathbf{r})], \tag{7}$$

where $\mathbf{h}$ is the diffraction vector.

Using these definitions, the distribution of the entire diffracted intensity (i.e., coherent *plus* diffuse parts) in reciprocal plane is given by[23]

$$J(q_x,q_z) = C\int_{-\infty}^{\infty} dq_y \int d\mathbf{r}\int d\mathbf{r}'\chi_h(z)\chi_h(z')\Omega(\mathbf{r})\Omega(\mathbf{r}') \times\Gamma(\mathbf{r}_\parallel-\mathbf{r}'_\parallel)\langle\Psi(\mathbf{r})\Psi^*(\mathbf{r}')\rangle \times\exp[2\pi i\mathbf{q}\cdot(\mathbf{r}-\mathbf{r}')], \quad (8)$$

where C is a constant and Γ is the mutual coherence function of the primary radiation, $\langle\,\rangle$ symbolizes a statistical averaging over all possible configurations of the random strains. We assume that the coherently irradiated area on the sample surface contains a sufficient number of dots, so that the waves emitted from different dots can interfere. The integration over the q_y component in Eq. (8) (perpendicular to the diffraction plane) is due to the very poor resolution of the diffractometer in the y direction.

The strain field has both nonrandom and random components,

$$\mathbf{u}(\mathbf{r}) = \langle\mathbf{u}(\mathbf{r})\rangle + \delta\mathbf{u}(\mathbf{r}), \quad (9)$$

and the mean value of Ψ can be expressed as

$$\langle\Psi(\mathbf{r})\rangle = E(\mathbf{r})\exp[2\pi i\mathbf{h}\cdot\langle\mathbf{u}(\mathbf{r})\rangle], \quad (10)$$

where

$$E(\mathbf{r}) = \langle\exp[2\pi i\mathbf{h}\cdot\delta\mathbf{u}(\mathbf{r})]\rangle \quad (11)$$

is the static Debye-Waller factor of the random part of the strain field. We assume that the nonrandom part of the strain field as well as the static Debye-Waller factor are the same for all dots. Consequently, $\langle\Psi(\mathbf{r})\rangle$ is a periodic function with respect to $\mathbf{r}_\parallel$. In the following, we will assume a constant Debye-Waller factor in the whole dot volume. Moreover, we neglect the transition region between the elastically relaxed MQW part of the dots and the nondeformed substrate part, and hence we assume that the elastic relaxation is homogeneous and the nonrandom deformation tensor is diagonal with constant components ε_{ii}.[2] Since we measure the shift $\langle\mathbf{u}(\mathbf{r})\rangle$ with respect to the substrate lattice, its components in the dot in position $\mathbf{R}$ are

$$\langle\mathbf{u}_\parallel\rangle = H_{\mathrm{MQW}}(z)(\mathbf{r}_\parallel-\mathbf{R})\varepsilon_{xx}, \quad \langle u_z\rangle = H_{\mathrm{MQW}}(z)(z-H_1)\varepsilon_{zz}. \quad (12)$$

The correlation properties of the random deformation field $\delta\mathbf{u}(\mathbf{r})$ are described by the covariance function,

$$Q(\mathbf{r}-\mathbf{r}') = \langle\{\exp[2\pi i\mathbf{h}\cdot\delta\mathbf{u}(\mathbf{r})]-E\} \times\{\exp[2\pi i\mathbf{h}\cdot\delta\mathbf{u}(\mathbf{r}')]-E\}^*\rangle. \quad (13)$$

The explicit form of the covariance Q depends on the defect model used. The simplest model introduced in our previous paper[11] (random deformation model) assumes that the random deformation field is described by a deformation tensor, whose random components have zero mean values and constant mean square deviations σ_{ij}^2. Here, we modified this model assuming no correlation of the random shifts in two different dots. Therefore, the assumed form of the covariance is

$$Q(\mathbf{r}-\mathbf{r}') = \begin{cases} (1-E^2)\exp[-2\pi^2(x_i-x'_i)(x_j-x'_j)a_{ij}^2], & \mathbf{r},\mathbf{r}' \text{ in the same dot} \\ 0, & \mathbf{r},\mathbf{r}' \text{ in different dots.} \end{cases} \quad (14)$$

The explicit expressions of the coefficients a_{ij} have been derived previously:[11]

$$a_{xx}^2 = h_x^2\sigma_{xx}^2 + h_z^2\sigma_{xz}^2, \quad a_{zz}^2 = h_x^2\sigma_{xz}^2 + h_z^2\sigma_{zz}^2, \quad a_{xz}^2 = h_xh_z\sigma_{xz}^2, \quad (15)$$

where $(h_x,0,h_z)$ are the coordinates of the diffraction vector $\mathbf{h}$. Since $h_y=0$, other terms of the matrix a_{ij} are zero.

A. Coherent part of the diffracted intensity

If the deformation field of the dot array has a random part, the diffracted beam can be divided in a coherent and an incoherent part. For the calculation of the coherent part, we replace the average $\langle\Psi\Psi^*\rangle$ by $\langle\Psi\rangle\langle\Psi\rangle^*$. Then, after some algebra, we get the following expression for the coherent part of the intensity distribution in the reciprocal plane,

$$J_C(q_x,q_z) = E^2C_1\sum_{\mathbf{G}}\Gamma^{\mathrm{FT}}(q_x-G_x)\left|\chi_h^{\mathrm{MQW}}\Omega_D^{\mathrm{FT}}(G_x+h_x\varepsilon_{xx},G_y)H_{\mathrm{MQW}}^{\mathrm{FT}}(q_z+h_z\varepsilon_{zz})+\chi_h^{\mathrm{sub}}\Omega_D^{\mathrm{FT}}(\mathbf{G})H_{\mathrm{sub}}^{\mathrm{FT}}(q_z)\right|^2, \quad (16)$$

where C_1 is a constant. From this equation it follows that the coherent intensity distribution in the q_xq_z-reciprocal plane exhibits maxima at the positions $q_x = G_x$ (lateral or dot satellites). The shape of these maxima is determined by the Fourier transformation Γ^{FT} of the coherence function of the primary beam, thus, their width is mainly given by the divergence of the primary beam. Their positions are determined by the lateral reciprocal lattice points and they are *not affected* by the deformation field $\langle\mathbf{u}(\mathbf{r})\rangle$. The intensities of the maxima, however, are influenced both by the averaged strains $\langle\mathbf{u}(\mathbf{r})\rangle$ and by the Debye-Waller factor E. $\langle\mathbf{u}(\mathbf{r})\rangle$ shifts the envelope function of these maxima by the vector $(-h_x\varepsilon_{xx},-h_z\varepsilon_{zz})$ in the q_xq_z-reciprocal plane, and E causes a decrease of the heights of all maxima. The point $(-h_x\varepsilon_{xx},-h_z\varepsilon_{zz})$ in the reciprocal plane is determined by the average lat-

tice constants of the dots. Its in-plane component $h_x\varepsilon_{xx}$ yields the average in-plane lattice constant $\langle a_D \rangle$ in the quantum dots. This is sketched schematically in Fig. 5. The vertical streaks are dot satellites both of the MQW part (SL_0) and the substrate part (S) of the dots. The gray scale indicates the relative intensities of the individual satellites. As shown in Fig. 5, both around symmetrical and asymmetrical diffraction peaks like (004) and $(\bar{2}\bar{2}4)$, the dot satellites of the substrate and the MQW share the same set of q_x coordinates. The in-plane lattice constant of the buffer layer $a_{\rm sub}$ determines the position of the sequence of the dot satellites for asymmetrical diffractions like $(\bar{2}\bar{2}4)$. Below this series, the analogous set of the dot satellites for the MQW part of the dots is shown. The symbol $\otimes$ denotes the maximum of the envelope function of the satellite intensities.

Thus, the position of the satellites in reciprocal space is *no measure* of the in-plane lattice constant in the nanostructures. The latter can only be obtained from the position of the envelope of the dot satellites.

In Sec. V, we will compare measured and calculated projections of the intensity distribution onto the q_x axis, i.e., an integration along the q_z direction. The coherent part of this projection is defined by

$$L_C(q_x) = \int_{-\infty}^{\infty} dq_z J_C(q_x, q_z), \tag{17}$$

and it does not depend on ε_{zz}.

B. Incoherent part of the diffracted intensity

The expression for the incoherent (diffuse) component of the diffracted intensity is identical to Eq. (8), if

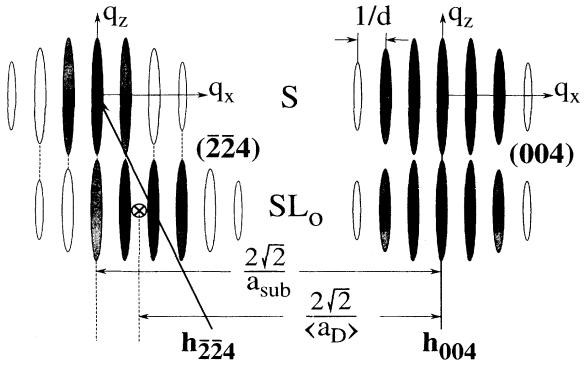

FIG. 5. Schematic sketch of the intensity distribution in the reciprocal plane close to (004) and $(\bar{2}\bar{2}4)$ reciprocal lattice points, $\otimes$ denotes the position of the reciprocal lattice point $(-h_x\varepsilon_{xx}, -h_z\varepsilon_{zz})$ of the dots, i.e., the maximum of the intensity envelope.

$\langle \Psi(\mathbf{r})\Psi^*(\mathbf{r}') \rangle$ is replaced by the covariance,

$$\langle \Psi(\mathbf{r})\Psi^*(\mathbf{r}') \rangle - \langle \Psi(\mathbf{r}) \rangle \langle \Psi(\mathbf{r}') \rangle^* = Q(\mathbf{r}-\mathbf{r}') \exp[2\pi i \mathbf{h}\cdot\{\langle \mathbf{u}(\mathbf{r}) \rangle - \langle \mathbf{u}(\mathbf{r}') \rangle\}]. \tag{18}$$

The diffusely scattered intensity is a sum of three components—the intensity originating in the MQW parts, in the substrate part of the dots, and in a damaged layer at the substrate surface.

The incoherent part of the diffracted intensity from MQW parts is given by

$$J_I^{\rm MQW}(q_x, q_z) = C_2 |\chi_h^{\rm MQW}|^2 \int\int d\kappa_x d\kappa_z Q^{\rm FT}(q_x + h_x\varepsilon_{xx} - \kappa_x, q_z + h_z\varepsilon_{zz} - \kappa_z) |H_{\rm MQW}^{\rm FT}(\kappa_z)|^2 |\Omega_D^{\rm FT}(\kappa_\parallel)|^2, \tag{19}$$

where C_2 is a constant, (κ_x, κ_z) is a variable position vector in the q_xq_z reciprocal plane, and $Q^{\rm FT}$ is the two-dimensional Fourier transform of the covariance function Q:

$$Q^{\rm FT}(\kappa_x, \kappa_z) = \int dx \int dz\, Q(x, 0, z) \exp[2\pi i(\kappa_x x + \kappa_z z)]. \tag{20}$$

If the characteristic correlation length of the random deformation field is much smaller than the size of the dots, then the Fourier transform of the correlation function $Q^{\rm FT}$ is nearly constant in the region, where the Fourier transform of the shape function $H_{\rm MQW}^{\rm FT}(\kappa_z)\Omega_D^{\rm FT}(\kappa_\parallel)$ appreciably differs from zero. The distribution of the diffusely scattered intensity in the reciprocal plane can be approximated by $Q^{\rm FT}$,

$$J_I(q_x, q_z) \approx \text{const}\ Q^{\rm FT}(q_x + h_x\varepsilon_{xx}, q_z + h_z\varepsilon_{zz}). \tag{21}$$

Similarly to the coherent case, the maximum of the diffuse scattering is shifted by $(-h_x\varepsilon_{xx}, -h_z\varepsilon_{zz})$. Since we have assumed no correlation of the random strains in different dots, the diffuse scattering distribution is only affected by the shape of the dots and hence it does not depend on the distribution of the dots in the dot array. Consequently, a completely random arrangement of the quantum dots would exhibit the same diffuse scattering, however, there would be just the central maximum, but no other coherent dot satellites.

The diffuse x-ray scattering coming from the substrate parts of the dots can be described by a formula similar to Eq. (19), where the shape function $H_{\rm MQW}^{\rm FT}$ is replaced by $H_{\rm sub}^{\rm FT}$ and the polarizability coefficient $\chi_h^{\rm MQW}$ by $\chi_h^{\rm sub}$. The shifts $\varepsilon_{xx}h_x$ and $\varepsilon_{zz}h_z$ are set to zero in this case, thus, this part of the diffuse scattering is concentrated around the substrate peak.

The damaged layer on the (001)-oriented substrate surface gives rise to diffuse scattering as well. Its distribution in the reciprocal plane is

$$J_I^{\rm sub}(q_x,q_z) = C_2|\chi_h^{\rm sub}|^2 \int d\kappa_z Q^{\rm FT}(q_x, q_z-\kappa_z) \times |H_{{\rm sub}L}^{\rm FT}(\kappa_z)|^2, \quad (22)$$

where

$$H_{{\rm sub}L}(z) = \begin{cases} 1 & \text{for } z \in (H_1+H_2, H_1+H_2+H_L) \\ 0 & \text{elsewhere} \end{cases}$$

is the shape function of the damaged layer on the substrate surface and H_L is its thickness.

In Sec. V, for the comparison of experimental and calculated results, we will use the projection of the incoherent intensity onto the q_x axis,

$$L_I(q_x) = \int_{-\infty}^{\infty} dq_z J_I(q_x,q_z). \quad (23)$$

This projection only depends on the coefficient a_{xx} of the covariance function.

V. DISCUSSION

In the first part of this section, we determine the dot radius R_D, the nonrandom deformation tensor components $\varepsilon_{xx,zz}$, as well as the coefficients $a_{xx,zz,xz}$ occurring in the covariance function Q from the measured RSM's. Then, using the theory outlined in the preceding section, we simulate the RSM's and compare them with the experimental data.

The analysis of the experimental data is somewhat hampered, because of the low diffuse intensity diffracted from the dots (less than 25 counts per sec). This fact made it impossible to compare directly the measured RSM's with the theory using a fitting procedure. In order to improve the signal-to-noise ratio, we calculated the projection,

$$L(q_x) = \int_{q_1}^{q_2} dq_z J(q_x,q_z), \quad (24)$$

of the measured RSM onto the q_x axis. The interval (q_1,q_2) has been chosen in a way that it covers only the coherent and diffuse peaks originating from the MQW part of the dots. The projections of the experimental maps around (004) and $(\bar{1}\bar{1}3)$ are shown in Figs. 6(a) and 6(b), respectively.

In the first step, we compare the positions and the heights of the coherent maxima of $L(q_x)$ with the theory. From the spacing of the dot satellites in reciprocal space, the periodicity of the dot array in the xz-incidence plane follows: $d = (3000 \pm 60)$ Å. This value coincides very well with the nominal one. A summary of all numerical values deduced from the RSM's and the simulations can be found in Table I.

The heights of the measured coherent maxima of $L(q_x)$ have been compared with the theoretical envelope function following from Eqs. (16) and (17). From this comparison (see Fig. 6), we obtained both the dot diameter R_D and the shift of the envelope caused by the nonrandom strain tensor element ε_{xx}. From the $L(q_x)$ function obtained from the $(\bar{1}\bar{1}3)$ and the (004) experimental RSM's, we found $R_D = (500 \pm 50)$ Å. This value is less than the nominal one (650 Å) and the difference can be assigned to the existence of a nondiffracting cylindrical layer at the sidewalls of the dots. From Fig. 6, the difference between the envelope function calculated for $R_D = 500$ Å [curve (1)] and that for $R_D = 650$ Å [curve (2)] is obvious. The curve (1) fits the coherent peaks

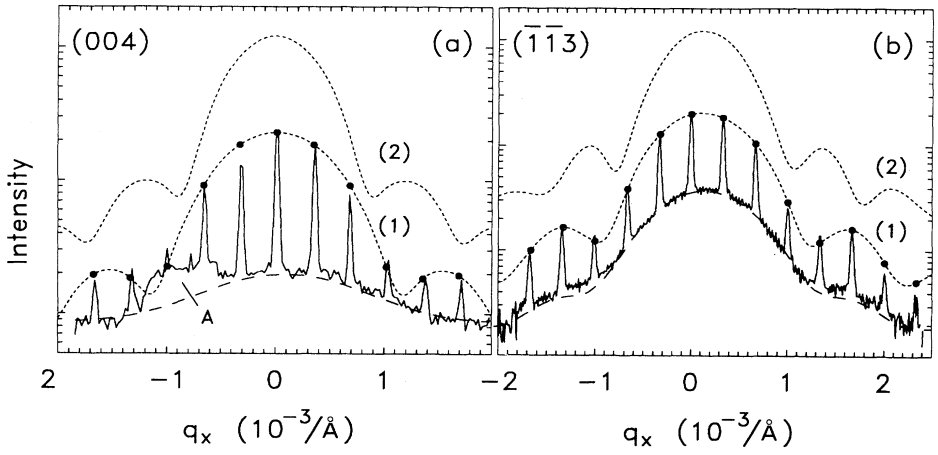

FIG. 6. Projection $L(q_x)$ of the measured RSM (full lines) around (004) (a) and $(\bar{1}\bar{1}3)$ (b). Full circles denote the positions and heights of the lateral satellites calculated for $R_D = 500$ Å, the dotted lines are the envelope functions calculated also for $R_D = 500$ Å [line (1)] and $R_D = 650$ Å (2). The lines (2) are shifted upwards by the factor of 10. The dashed line is the best fit of the incoherent intensity distribution on which the coherent intensity is superimposed. In (a), the peak denoted "A" is the projection of the analyzer streak.

TABLE I. Structural parameters of the dot array obtained from the RSM's.

	Nominal value	(004) coherent	(004) diffuse	$(\bar{1}\bar{1}3)$ low exit coherent	$(\bar{1}\bar{1}3)$ low exit diffuse	(113) low incidence coherent	(113) low incidence diffuse
d (Å)	3000	3000±60		3000±60		3000±60	
R_D (Å)	650	500±50		500±50	520±70	500±50	
$10^4\varepsilon_{xx}$				5±1	5.0±0.6	5±1	4.3±0.8
$10^3\varepsilon_{zz}$	0.734[a]		2.0±0.2		2.4±0.2		2.5±0.3
$10^3 a_{xx}$ (Å^{-1})			3±1		1.3±0.1		1.3±0.3
$10^3 a_{zz}$ (Å^{-1})			0.7±0.3		1.3±0.3		0.9±0.2
$10^3 a_{xz}$ (Å^{-1})			0		1.0±0.2		-1.1±0.3

[a] ε_{zz}^{max}–see Sec. V.

much better than the curve (2).

The shift of the experimental projection curve $L(q_x)$ in $(\bar{1}\bar{1}3)$ diffraction yielded the relative difference in the in-plane lattice constants of the MQW part of the layers and the substrate $\varepsilon_{xx} = (5 \pm 1)10^{-4}$. The projection curve of the (004) diffraction is symmetrical with respect to $q_x = 0$, since $h_x = 0$ holds in this case.

The diffuse parts of the measured projections $L(q_x)$ have been compared with the theory using Eqs. (19) and (23). From this comparison, we found the same value of ε_{xx} as from the coherent peaks. The projections of the incoherent intensity yielded the coefficient a_{xx} of the covariance function. Since this coefficient contains the components of the diffraction vector $\mathbf{h}$, its values are different for $(\bar{1}\bar{1}3)$ and (004) diffractions. The following values have been found: $a_{xx} = (1.3\pm0.1)10^{-3}$ Å^{-1} for $(\bar{1}\bar{1}3)$ and $a_{xx} = (3 \pm 1)10^{-3}$ Å^{-1} for (004). The larger statistical error of (004) is due to the fact that the RSM, (004) has been measured using an analyzing crystal and, therefore, the intensity was lower than in the $(\bar{1}\bar{1}3)$ RSM, which has been acquired with a slit in front of the detector. The low noise in the $(\bar{1}\bar{1}3)$ data allowed us to determine the dot radius R_D from the diffusely scattered intensity, we obtained $R_D = (520 \pm 70)$ Å, which agrees very well with the value following from the envelope of the coherent satellite peaks. From that fact it follows that the whole dot volume is the source of the diffusely scattered intensity and, therefore, the random strains are extended through the entire dots. The shape of the theoretical projection $L_I(q_x)$ coincides quite well with the measurement [see Figs. 6(a), 6(b)]. The hump in the measured (004) projection denoted by "A" in Fig. 6(a) corresponds to the analyzer streak[8] caused by the analyzing crystal in the triple-axis arrangement.

The parameters ε_{zz}, a_{xz}, and a_{zz}, cannot be obtained from the projections $L(q_x)$, they have to be obtained from the whole RSM's. The relative difference ε_{zz} of the MQW and substrate lattice constants has been determined from the position of the centers of the broad diffuse intensity distributions. From the experimental maps, we obtained the values $\varepsilon_{zz} = (2.4 \pm 0.2)10^{-3}$ for $(\bar{1}\bar{1}3)$ and $\varepsilon_{zz} = (2.0 \pm 0.2)10^{-3}$ for (004). The coefficient a_{xz} was determined from the $(\bar{1}\bar{1}3)$ diffraction, since it is zero for (004). This coefficient is responsible for the rotation of the isointensity contours of the diffusely scattered intensity with respect to q_x axis and its value is $a_{xz} = (1.0 \pm 0.2)10^{-3}$ Å^{-1}. The value of a_{zz} follows from the width of the diffuse intensity distribution in q_z direction. From the RSM's, we obtained $a_{zz} = (1.3 \pm 0.3)10^{-3}$ Å^{-1} for $(\bar{1}\bar{1}3)$ and $a_{zz} = (0.7 \pm 0.3)10^{-3}$ Å^{-1} for (004).

Using these values, we calculated the intensity distributions in the reciprocal plane for both the (004) and the $(\bar{1}\bar{1}3)$ reflections, the results can be seen in Figs. 3(b) and 4(b). In these calculations, we neglected the contributions of the substrate "necks" of the dots, as well as the damaged layer on the substrate surface, and therefore, only the intensity distribution around the SL_0 peak was simulated. The experimental and simulated distributions compare quite well as shown in Figs. 3 and 4.

The diffuse scattering taking place in the region with the GaAs substrate lattice parameter, i.e., both in the "necks" of the dots and in a damaged layer at the substrate surface between the dots, can only be measured by means of an analyzing crystal, since it cannot be resolved from the substrate peak if we use only the detector slit. The result of this measurement close to the (113) reciprocal lattice point (low angle of incidence) is shown in Fig. 7(a). Similarly to Fig. 4, from the shape of the MQW diffuse scattering peak, we determined both the elastic relaxation parameters $\varepsilon_{xx,zz}$ and the random strain coefficients a_{ij}. In the error limits, we found the same values of the coefficients ε_{xx}, ε_{zz}, a_{xx}, and a_{xz} as those from Fig. 4(a) (see Table I), only the value of $a_{zz} = (0.9 \pm 0.2)10^{-3}$ is slightly smaller than that from Fig. 4(a). The difference is caused by the resolution function of the diffractometer. We measured the map in Fig. 4(a) using the slit in front of the detector, while the map in Fig. 7(a) has been obtained by a triple-crystal arrangement. From the width of the detector slit and its distance from the sample, it follows that the resolution function in the former case is broadened along the Ewald sphere by approximately 2×10^{-4} Å^{-1}. For $(\bar{1}\bar{1}3)$ and Cu $K\alpha$ radiation, this Ewald sphere is nearly parallel to the q_z axis.

An interesting feature is that the diffuse scattering peak around the substrate peak is substantially more rotated with respect to the q_x axis than the diffuse scattering originating from the etched MQW and, in addition, the center of the peak is shifted in negative q_z direction (see Fig. 7). From this shift it follows, that the damaged area in the substrate structure is nonrandomly tetrago-

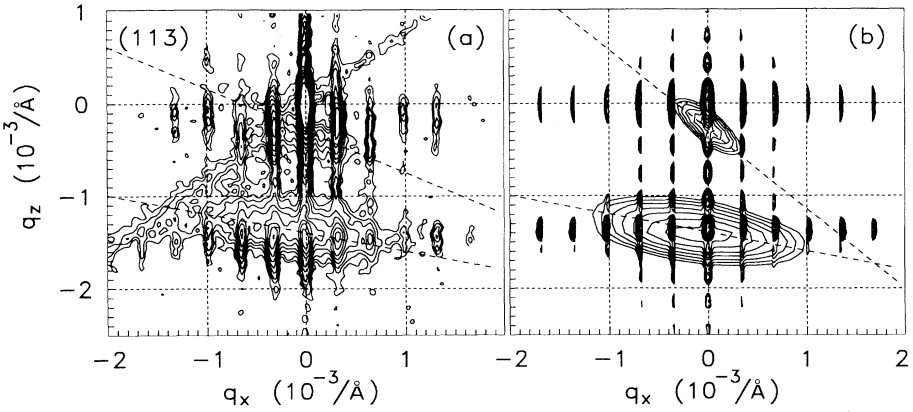

FIG. 7. Measured (113) RSM (low angle of incidence) showing diffuse scattering, which originates both in the GaAs substrate and the MQW structure (a). Simulation (b) using the same set of parameters as determined from the diffuse scattering of the etched MQW. The dashed lines indicate the orientation of the principal axis of the broad diffuse scattering peaks.

nally strained. Its mean in-plane lattice parameter remains $a_{\rm sub}$, while the vertical one is larger by approximately $4.5 \times 10^{-4} a_{\rm sub}$. In the simulation [Fig. 7(b)], we took the same set of parameters as that determined from the diffuse scattering coming from the MQW structure. The larger rotation of the peak substrate peak, with respect to the q_x axis, is caused by different shapes of the damaged regions both in the neck parts of the dots, as well as in the unstructured part of the substrate, and in the MQW parts. The rotation is well reproduced by the simulation, it is slightly larger than in the measurement. The sense of the rotation of the MQW diffuse scattering peak is opposite to that in Fig. 4(a). It is caused by the opposite diffraction asymmetry (low angle of incidence).

So far, we do not know, why this diffuse scattering from the substrate is not visible in the (004) RSM. One reason may be that the penetration depth of the x rays into the substrate is much larger at (004) (approximately 16 μm) than at (113) (approximately 1.5 μm), and therefore the relative contribution of the damaged surface layer is weaker. Another possible reason for the absence of the diffuse scattering in the (004), RSM is the fact that the areas illuminated by the primary beam are different. Whereas for (004), ω is about 33° and the x-ray spot size is 2 mm × 9 mm, for (113) $\omega \approx 1.6°$ and the illuminated area covers the whole sample area of 9 mm × 20 mm. In the latter case, also the unstructured parts, where all the MQW has been etched away, are hit by x rays. Possibly, in these parts the random elastic deformations are different from the ones in the structured regions.

From our theoretical description it follows that the position of the lateral satellites does not depend on the deformation field in the dots. This conclusion is a consequence of the assumption that the nonrandom part of the deformation field is same in all dots, thus the averaged phase function $\langle \Psi \rangle = \langle \exp[i\mathbf{h} \cdot \mathbf{u}(\mathbf{r})] \rangle$ has the same period as the dot array. This consideration is only valid for lateral structures fabricated in pseudomorphic layers, i.e., only for elastic relaxation of internal strains. If the layered structure were plastically relaxed (i.e., due to dislocations) before etching the dot structure, the averaged phase function $\langle \Psi \rangle$ would not be periodic and the dot satellites could be shifted laterally. Therefore, the in-plane *elastic* relaxation of the internal strains in the dots and, consequently their mean in-plane lattice parameter, can only be investigated from the shift of the *envelope function* of the satellites. The envelope function projected onto the q_x axis does not depend on the vertical elastic strain relaxation even in the case of a nonhomogeneous distribution of ε_{zz}.

In order to study the vertical relaxation, the dependence of the intensity of the lateral satellites on q_z must be taken into account. A detailed inspection of this intensity dependence showed that it differs appreciably from that for constant ε_{zz} and, moreover, is different for different satellite orders. Therefore, the elastic relaxation of the internal strains is not homogeneous in our sample and, consequently, $\varepsilon_{zz}, \varepsilon_{xx}$ values found above only represent effective mean values of the actual $\varepsilon_{ij}(\mathbf{r})$ distributions. Most probably, this fact is the reason why the values of ε_{zz} found from the (004) and the $(\bar{1}\bar{1}3)$ diffraction differ.

The maximum elastic relaxation of the dot structure is given by

$$\varepsilon_{zz}^{\rm max} = \frac{a_{\rm MQW} - a_{\rm sub}}{a_{\rm sub}}, \tag{25}$$

where $a_{\rm MQW}$ is the lattice parameter of the unstrained MQW structure,

$$a_{\rm MQW} = \frac{a_{\rm GaAs} t_{\rm GaAs} + a_{\rm AlAs} t_{\rm AlAs}}{t_{\rm GaAs} + t_{\rm AlAs}}, \tag{26}$$

$a_{\rm GaAs} = a_{\rm sub}$ and $a_{\rm AlAs}$ are the *bulk* lattice constants of both materials and $t_{\rm GaAs}, t_{\rm AlAs}$ are their thicknesses. For our structure, $\varepsilon_{zz}^{\rm max} = 7.34 \times 10^{-4}$. The measured vertical deformation ε_{zz} is larger than $\varepsilon_{zz}^{\rm max}$, thus, this deformation is caused not only by the relaxation of the internal strains due to the lattice mismatch. Possible explanations of this discrepancy are the implantation of foreign ions into the dot structure, during the reactive ion etching or an additional strain caused by oxidation of the sidewalls of the AlAs layers.

From the envelope function of the lateral satellites, as well as from the distribution of the diffusely scattered intensity, it follows that the radius of the dots is smaller than that obtained from SEM micrographs. Thus, some nondiffracting (heavily distorted) cylindrical layer with a

thickness of about 150±50 Å occurs close to the sidewalls of the dots. Most likely, this layer was produced during the reactive ion etching of the structure.

However, even the crystalline core of the dots is not perfect, it gives rise to diffuse x-ray scattering, its distribution in reciprocal plane can be explained by means of the random deformation model. The values of the coefficients a_{xx}, a_{zz}, and a_{xz} occurring in the correlation function Q have been obtained with large errors and, in addition, were influenced by the worse resolution of the detector slit in the case of the $(\bar{1}\bar{1}3)$ RSM. These facts do not permit us to determine the root-mean-square deviations of the random strains, a rough estimate of these deviations yields a value of 3×10^{-4} with uncertainty of about 100%.

Our model of the structure of the dots (amorphous surface layer and crystalline, randomly strained core) is only a rough description of the actual structure. Most likely, the degree of crystalline order expressed by the static Debye-Waller factor E continuously decreases in the radial direction towards the surface to zero in the heavily distorted layer and, thus there is no abrupt boundary between the crystalline and distorted parts as indicated by the gray scale in Fig. 1.

VI. CONCLUSIONS

We have studied the structural properties of a AlAs/GaAs multiple quantum periodic dot array (defined by electron beam lithography and fabricated by reactive ion etching) by means of high-resolution x-ray reciprocal space mapping. From the envelope function of the dot satellites, we derived the averaged in-plane lattice constant, as well as the radius of the crystalline core of the dots. We explained the shape of the envelope function by means of a structure model, assuming the presence of a heavily distorted cylindrical layer close to the sidewalls of the dots, and we determined the thickness of this layer. However, this model is apparently an approximation and most likely, in the actual structure, the degree of crystallinity decreases radially from the center towards the outer surfaces of the dot structures.

Diffuse x-ray scattering accompanying the SL_0 coherent intensity gave the evidence for the presence of a random strain field extending throughout the whole crystalline dot volume. In addition, we observed diffuse x-ray scattering around the substrate peak, which indicates random strains in the substrate part of the dots and in a layer on the GaAs substrate surface. The distribution of the diffusely scattered x-ray intensity in reciprocal plane has been simulated using the random deformation model and a good agreement with the experiments has been achieved.

ACKNOWLEDGMENTS

This work has been supported by the Bundesministerium für Wissenschaft und Forschung (Project No. GZ 601.540/1-26/92), by the Gesellschaft für Mikroelektronik (Project No. P VI/94), by the Engineering Physical and Science Research Council (UK) (Grant No. GR/J90718), and by the Grant Agency of Czech Republic (Grant No. 202/94/1871). We are grateful to H. Straub and to A. Ross for technical assistance.

* Permanent address: Department of Solid State Physics, Faculty of Science, Masaryk University, 61137 Brno, Czech Republic.

[1] H. Benisty, C. M. Sotomayor Torres, and C. Weisbuch, Phys. Rev. B **44**, 10 945 (1991).
[2] L. De Caro and L. Tapfer, Phys. Rev. B **49**, 11 127 (1994).
[3] L. Tapfer and P. Grambow, Appl. Phys. A **50**, 3 (1990).
[4] A. T. Macrander and S. E. G. Slusky, Appl. Phys. Lett. **56**, 443 (1990).
[5] V. Holy, L. Tapfer, E. Koppensteiner, G. Bauer, H. Lage, O. Brandt, and K. Ploog, Appl. Phys. Lett. **63**, 3140 (1993).
[6] P. v. d. Sluis, M. J. Verheijen, and J. Haisma, Appl. Phys. Lett. **64**, 3605 (1994).
[7] A. Iida and K. Kohra, Phys. Status Solidi A **51**, 533 (1979).
[8] P. F. Fewster, Semicond. Sci. Technol. **8**, 1915 (1993).
[9] M. A. Krivoglaz, *Theory of X-Ray and Thermal Neutron Scattering by Real Crystals* (Plenum, New York, 1969).
[10] A. A. Lomov, P. Zaumseil, and U. Winter, Acta Crystallogr. Sec. A **41**, 223 (1985).
[11] V. Holý, K. Wolf, M. Kastner, H. Stanzl, and W. Gebhardt, J. Appl. Crystallogr. **27**, 551 (1994).
[12] *Nanostructure Physics and Fabrication*, edited by M. A. Reed and W. P. Kirk (Academic Press, Boston, 1989).
[13] *Nanostructures and Mesoscopic Systems*, edited by W. P. Kirk and M. A. Reed (Academic Press, Boston, 1992).
[14] H. Qiang, F. H. Pollak, Y. S. Tang, P. D. Wang, and C. M. Sotomayor Torres, Appl. Phys. Lett. **64**, 2830 (1994).
[15] E. M. Clausen, H. G. Craighead, J. P. Harbison, A. Scherer, L. M. Schiavone, B. V. d. Gaag, and L. T. Florez, J. Vac. Sci. Technol. B **7**, 2011 (1989).
[16] K. Kash, B. P. v. d. Gaag, D. Mahoney, A. S. Gozdz, L. T. Florez, J. P. Harbison, and M. D. Sturge, Phys. Rev. Lett. **67**, 1326 (1991).
[17] I.-H. Tan, D. Lishan, R. Mirin, V. Jayaraman, T. Yasuda, E. L. Hu, and J. Bowers, Appl. Phys. Lett. **59**, 1875 (1991).
[18] C. M. Sotomayor Torres, W. E. Leitch, D. Lootens, P. D. Wang, G. M. Williams, S. Thoms, H. Wallace, P. Van Daele, A. G. Cullis, C. R. Stanley, P. Demeester, and S. P. Beaumont, in *Nanostructures and Mesoscopic Systems* (Ref. 13), pp. 455–461.
[19] P. D. Wang, M. A. Foad, C. M. Sotomayor Torres, S. Thoms, M. Watt, R. Cheung, C. D. W. Wilkinson, and S. P. Beaumont, J. Appl. Phys. **71**, 3754 (1992).
[20] P. D. Wang and C. M. Sotomayor Torres, J. Appl. Phys. **74**, 5047 (1993).
[21] Y. P. Song, P. D. Wang, C. M. Sotomayor Torres, and C. D. W. Wilkinson, J. Vac. Sci. Technol. B **12**, 3388 (1994).
[22] M. Gailhanou, T. Baumbach, U. Marti, P. C. Silva, F. K. Reinhart, and M. Ilegems, Appl. Phys. Lett. **62**, 1623 (1993).
[23] J. M. Cowley, *Diffraction Physics* (North-Holland, Amsterdam, 1975).

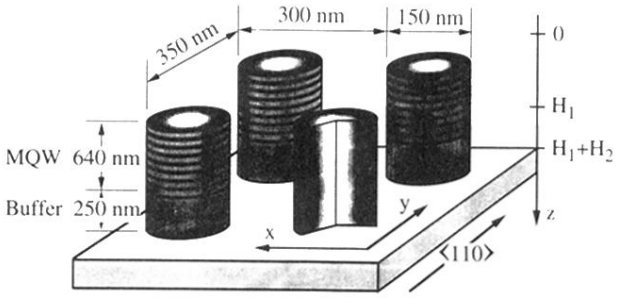

FIG. 1. Schematic diagram of the periodic GaAs/AlAs dot array.

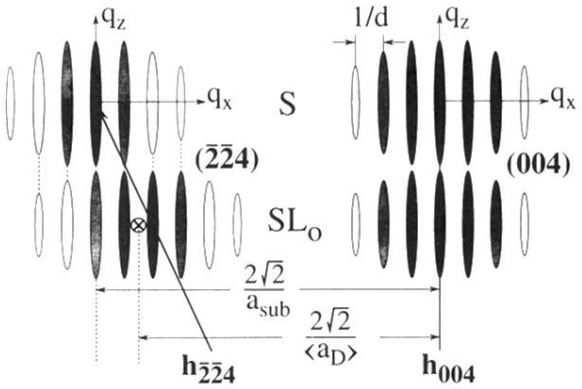

FIG. 5. Schematic sketch of the intensity distribution in the reciprocal plane close to (004) and $(\bar{2}\bar{2}4)$ reciprocal lattice points, $\otimes$ denotes the position of the reciprocal lattice point $(-h_x\varepsilon_{xx}, -h_z\varepsilon_{zz})$ of the dots, i.e., the maximum of the intensity envelope.